Extended Abstracts of the 2017 International Conference on Solid State Devices and Materials, Sendai, 2017, pp291-292

F-5-01

The Super-Nernstian pH-sensitivity of CeY_xO_y Sensing Membrane Electrolyte–Insulator–Semiconductor Sensors

Chi-Lin Chan, Yen-Hsiang Huang, Chih-Wei Wang, and Tung-Ming Pan*

Department of Electronic Engineering, Chang Gung University, 259, Wenhua 1st Rd., Guishan Dist. Taoyuan, Taiwan 33302
Tel: +886-3-211-8800 ext. 3349, Fax:+886-3-211-8507, Email:tmpan@mail.cgu.edu.tw

Abstract

In this paper we developed CeY_xO_y sensing membranes displaying super-Nernstian pH-sensitivity for use in electrolyte–insulator–semiconductor (EIS) pH sensors. We attribute the super-Nernstian pH-sensitivity to the incorporation of Y ions in the Ce framework, thereby decreasing the oxidation state Ce ($Ce^{4+}\rightarrow Ce^{3+}$) and resulting in less than one electron transferred per proton in the redox reaction.

1. Introduction

Rare earth (RE) oxide films are possible replacements for traditional SiO_2 as the gate dielectric in advanced CMOS devices [1-2]. Among them, CeO_2 thin films have several advantages, including strong adhesion, high refractive index, good redox, high mechanical strength, excellent thermal stability [3-4]. The major concern when using RE oxide films as sensing membranes, however, is prone to moisture absorption, which degrades permittivity through the formation of low-permittivity hydroxides. To address this issue, several researchers in literatures [5-6] have reported the incorporation of other elements (e.g., Ti, TiO_x, Y) into RE dielectric films which suppress the moisture absorption of the RE oxide.

2. Device Fabrication

A ~60 nm CeY_xO_y film was deposited on the Si substrate through rf co-sputtering from CeO_2 and Y targets. The samples were subjected to rapid thermal annealing (RTA) in O_2 ambient for 30 s at 600, 700, 800, or 900 °C to achieve a crystalline $(CeY)O_2$ film. To define the sensing area of the deposited CeY_xO_y, an automatic robotic dispenser was used with an adhesive silicone gel acting as a segregating layer. The EIS sensor was assembled on a Cu wire on a custom-made PCB by silver glue. The structure of the fabricated CeY_xO_y EIS device is illustrated in Fig. 1.

3. Results and Discussion

Fig. 2 shows that the surface roughness (rms) values of 1.77, 1.81, 1.92, and 252 nm were determined for the CeY_xO_y films treated at 600, 700, 800, and 900 °C, respectively. It can be see that the surface roughness value increased with increasing the annealing temperature.

In Fig. 3, we show the XRD patterns of CeY_xO_y sensing films annealed at different temperatures. The diffraction peaks of all the films assigned to the (111), (200), (220), and (311) planes are indexed to the face-centered cubic structure of $(CeY)O_2$ crystals. A strong $(CeY)O_2$ (111) peak, $(CeY)O_2$ (200) peak, and two weak $(CeY)O_2$ (220) and (311) peaks appeared in the patterns of the samples that had been annealed at 800 and 900 °C, suggesting the formation of a stoichiometric $(CeY)O_2$ film.

The Ce $3d_{5/2}$ spectra in Fig. 4(a) can be deconvoluted into three peaks: v (~882.6 eV), v' (~884.7 eV) and v'' (~888.9 eV). The $3d^{10}4f^0$ state of Ce^{4+} species are labeled as v and v'', whereas the $3d^{10}4f^1$ state of Ce^{3+} is represented as v' [7]. Fig. 4(b) displays that the positions of the Y $3d_{3/2}$ and $3d_{5/2}$ peaks shifted to higher binding energies upon increasing the annealing temperature. Fig. 4 (c) presents the O 1s spectra for the annealed CeY_xO_y films, with appropriate curve-fitting of the peaks. In the three spectra, the O 1s peaks at 533.4, ~531.5, and ~530.6 eV represent the Ce–OH, Ce–O–Y, and Ce–O bonds, respectively. The intensity of the O 1s peak corresponding to $(CeY)O_2$ increased upon increasing the RTA temperature—except at 900 °C, where it decreased relative to the signal for Ce_2O_3. This behavior suggests that Ce and Y atoms reacted with O atoms to form a stoichiometric $(CeY)O_2$ film.

Figs. 5(a)–(d) display the pH-dependence of a group of C–V curves for the CeY_xO_y EIS devices annealed at various temperatures. The insets to Figs. 5 (a)–(d) display the V_{REF} as function of pH values for the CeY_xO_y EIS devices after annealing at various temperatures. The pH-sensitivities of the CeY_xO_y films after RTA at 600, 700, 800, and 900 °C were determined to be 59.98, 62.77, 78.15, and 73.68 mV/pH, respectively. The CeY_xO_y EIS device annealed at 800 °C exhibited the highest sensitivity, possibly suggesting the higher surface roughness (AFM) of its CeY_xO_y sensing film. A higher surface roughness will increase the surface site density. Moreover, the pH-responses for the CeY_xO_y EIS sensors were higher than that expected (59.6 mV/pH) from the Nernst law, possibly because the addition of Y ions into the Ce framework enhanced the decrease in the Ce oxidation state ($Ce^{4+}\rightarrow Ce^{3+}$). During the oxygen release process, the volume of the Ce compound increases in proportion to the change in the Ce oxidation state from Ce^{4+} to Ce^{3+}. The introduction of Y ions into the Ce framework would compensate for the increase in volume and ease the change in valence of the Ce oxidation state. Fig. 6 presents the hysteresis voltages of CeY_xO_y EIS devices annealed at various temperatures. The EIS sensor annealed at 800 °C exhibited the smallest hysteresis voltage (1.4 mV), while that annealed at 600 °C had the highest (126.3 mV). Fig. 7 displays the drift characteristics of the CeY_xO_y EIS devices annealed at the various RTA temperatures. The CeY_xO_y EIS device annealed at 800 °C had the best long-term stability (0.85 mV/h), while the device annealed at 600 °C exhibited a serious drift rate (7.40 mV/h).

3. Conclusions

We observed a super-Nernstian response to pH from EIS devices incorporating CeY_xO_y sensing membranes grown on Si substrates. XRD, XPS, and AFM confirmed the presence of $(CeY)O_2$ structures in these EIS devices.

The CeY_xO_y EIS device annealed at 800 °C was the best pH-sensing performance among these temperatures. This enhanced performance stemmed from the formation of a stoichiometric $(CeY)O_2$ film, a high surface roughness, and a low number of crystal defects. The super-Nernstian pH-response appears to have resulted from the Y ions incorporated within the Ce framework enhancing the valence change of the Ce oxidation state, thus causing less than one electron to be transferred per proton in the redox reaction.

Acknowledgment

The authors would like to thank the Ministry of Science and Technology of Taiwan for financially supporting this research under contract of MOST-105-2111-E-182-064.

References

[1] T. M. Pan and K. M. Liao, Sen. Actuators B 128 (2007) 245.
[2] O. Engstrom, et al., Solid State Electron. 51 (2007) 622.
[3] X. Q. Fu, et al., Nanotechnology18 (2007) 145503.
[4] N. Izu et al., Solid-State Lett. 10 (2007) J37.
[3] K. Nomura et al., Science 300 (2003) 1269.
[4] E. Fortunato et al., Adv. Mater. 24 (2012) 2945.
[5] Y. Zhao et al., Appl. Phys. Lett. 89 (2006) 252905.
[6] T. Schroeder, et al., Appl. Phys. Lett. 87 (2005) 022902.
[7] B. M. Reddy, et al., Langmuir 19 (2003) 3025.

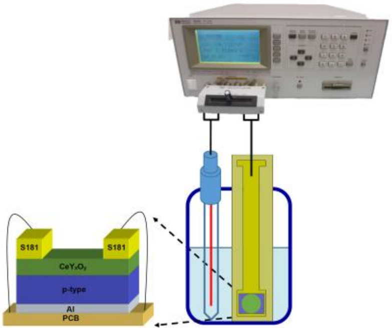

Fig. 1. Schematic representation of the structure of a CeY_xO_y EIS sensor.

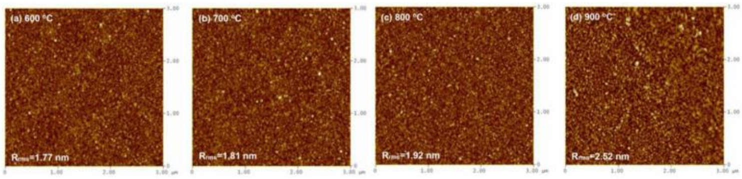

Fig. 2. AFM images of CeY_xO_y films sensing films annealed at (a) 600, (b) 700, (c) 800, and (d) 900 °C.

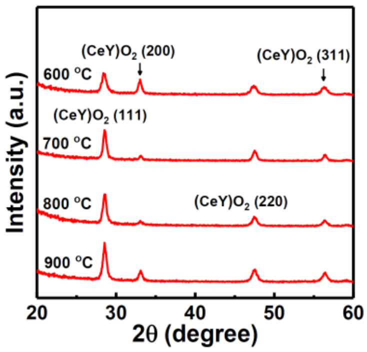

Fig. 3. XRD patterns of CeY_xO_y films annealed at various temperatures.

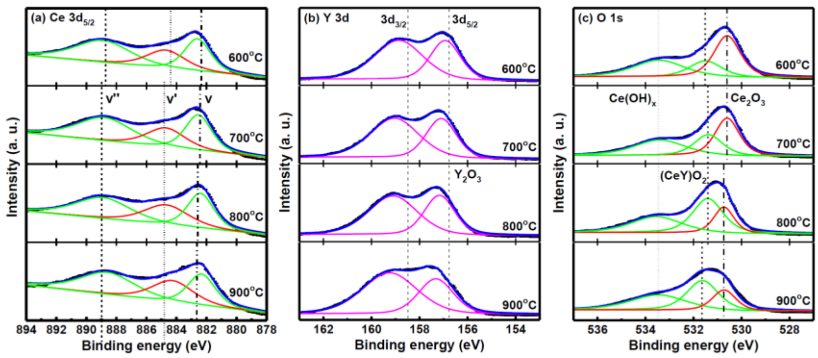

Fig. 4. XPS spectra displaying the (a) Ce 3d, (b) Y 3d, and (c) O 1s energy levels in CeY_xO_y films annealed at various temperatures.

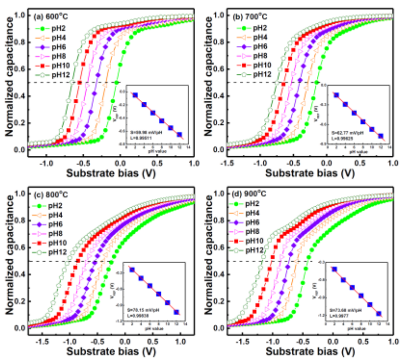

Fig. 5. Responses of the *C*–*V* curves for CeY_xO_y EIS sensors annealed at (a) 600, (b) 700, (c) 800, and (d) 900 °C. Insets: Reference voltages plotted with respect to pH for the CeY_xO_y EIS sensors.

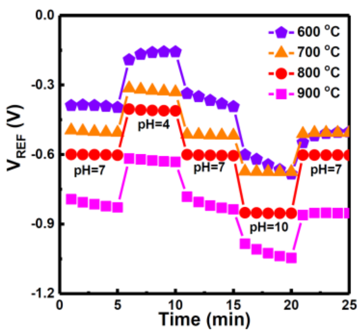

Fig. 6. Hysteresis voltages during the pH loop 7→4→7→10→7 of CeY_xO_y EIS devices after annealing at various temperatures.

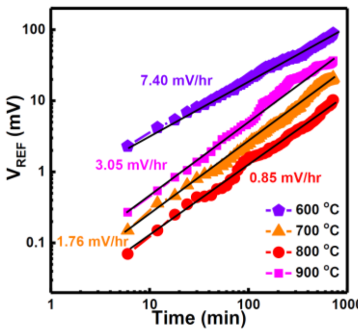

Fig. 7. Drift rates measured in solution at pH 7 of CeY_xO_y EIS sensors after annealing at various temperatures.